

Maximizing Synchronous Condensers' Capability to Stabilize Inverter-Based-Resource-Penetrated Grids

Li Bao, *Member, IEEE*, Lingling Fan, *Fellow, IEEE*, Zhixin Miao, *Senior Member, IEEE*

Abstract—Synchronous condensers (SynCons) have been deployed in power grids penetrated by inverter-based resources (IBRs) worldwide to strengthen and stabilize the grids. This paper examines which machine parameters influence IBR weak grid stability and whether excitation systems also play a role. Four types of stability scenarios are examined, including transient stability, oscillations of a few Hz, oscillations near 9 Hz, and dynamic voltage stability. It is shown that the most influential machine parameter varies for the different types of stability issues. While minimization of field winding inductance (typically the major component of the machine transient reactance, X'_d) can significantly improve transient stability, voltage stability, and low-frequency oscillatory stability, this parameter has no influence on relatively rapid oscillations. On the other hand, minimizing rotor damper winding inductance (typically the major component of the machine subtransient reactance, X''_d) improves the 9-Hz oscillation stability, but with insignificant influence on the other three types of stability. Furthermore, the excitation system characteristics show negligible influence for any of the scenarios. In addition to the simulation studies, we show how the operational reactances are associated with the machine's dq impedance viewed from the terminal bus and how a SynCon reduces the equivalent grid impedance, thereby improving weak grid stability. Finally, it is concluded that minimization of both transient and subtransient direct-axis reactances should help in a range of stability scenarios, while cautions should be taken when dealing with quadrature-axis transient reactances.

Index Terms—Synchronous condenser, weak grid, wind farm, IBR system, excitation system

I. INTRODUCTION

WITH the increasing penetration of IBR systems and the retirement of the traditional generators, the power system is experiencing declining system inertia and reduced grid strength. A power system of low inertia is likely to experience frequency and angular instability after contingency events and may result in blackouts [1]. Moreover, the IBR systems are usually installed in remote areas without synchronous generators. Such areas have a low Short Circuit Ratio (SCR) and are termed as weak grids. The grid industry has cautioned IBR integration in weak grids. According to a guideline published by North American Electric Reliability Corporation (NERC) [2], there are two types of stability risks. First, reduced grid strength leads to high sensitivity of voltage towards real and reactive power injection, and thus increasing the risk of voltage stability as well as control interactions. Second, reduced grid strength also leads to phase-locked-loop (PLL) stability issues during or after faults. The combination of low inertia and low SCR have led to real-world IBR

dynamic events, as documented by event analysis reports from NERC (e.g., [3]) and IEEE PES IBR SSO task force papers [4], [5].

In many real-world IBR oscillation events, IBR real power curtailment is usually adopted to mitigate stability issues. However, this method only serves as a contingent operating practice. For weak grid voltage stability enhancement, improved IBR controls, e.g., adopting fast voltage control and reducing voltage sensitivity [6], adopting grid-forming control [7], is an economic option.

Aiming for both frequency and voltage stability enhancement, the grid is seeking for technologies such as grid forming IBRs, STATCOMs, and SynCons. Both STATCOMs and SynCons have been adopted for IBR grid integrated systems for voltage support. Most recently, a 345 kV, ± 167 MVAR STATCOM has been installed at the Tewksbury substation to facilitate offshore wind farm grid integration in Eversource.

Compared to power electronic converter-based STATCOMs, SynCons require higher construction and maintenance costs. An advantage of SynCons is that this is a mature technology and SynCons can be built by retrofitting old generators. In 2019, Australia installed a 190 MVA SynCon in the 200 MW Kiamal Solar Farm, which improved the voltage oscillation observed in the system test [8]. In 2018, two SynCons with rated capacity of +175/-125 MVA were installed in Texas Panhandle area, where wind generation capacity accounts for majority of total generation [9]. The installation helped increase 400 MW more power exporting level from 3100 MW in 2017. ERCOT is currently evaluating installing SynCons in the west Texas region with 34.5 GW IBRs to avoid similar disturbances as the 2021 Odessa events [10]. It is found that 2.45 GW SynCons can help improve the grid strength by 16%.

Our prior research has also shown that even a SynCon supplies zero reactive power, it still helps IBR weak grid stability [11]. The major finding is that compared to a STATCOM in grid-following control mode which acts as a pure current source, a SynCon provides additional shunt reactance in the low to subsynchronous frequency region. This reactance makes the equivalent Thévenin grid impedance smaller. Thus, the grid appears stronger to the IBR. It is also found from [11] that at the approximate 1-Hz region, the provided reactance by the SynCon is much less than the steady-state d -axis reactance X_d while closer to the transient d -axis reactance X'_d .

A. Goals and Contributions

In this article, we further investigate which machine parameters are most sensitive for stability enhancement. This investigation has a high practical value by providing a guideline of

L. Bao is with Eversource. L. Fan, and Z. Miao are with University of South Florida. Email: linglingfan@usf.edu.

parameter selection or SynCon manufacturing. For example, through adjusting a SynCon's winding parameters, a SynCon can have improved performance.

To this end, this article relies on electromagnetic transient (EMT) simulation to examine which machine winding parameters mostly influence stability and whether excitation systems also play a role. Our focus is IBR weak grid stability issues usually in the subsynchronous frequency range below 20 Hz. Four types of stability scenarios are examined, including transient stability, dynamic voltage stability, oscillations at 2-4 Hz, and oscillations at 9 Hz. It is seen that for different types of stability issues, the most influential machine parameter is also different. While reduction in the field winding inductance can significantly improve transient stability, dynamic voltage stability, and low-frequency oscillation stability, this has no influence on the 9-Hz oscillation stability. On the other hand, reduction in the damping winding inductance improves the 9-Hz oscillation stability, while showing insignificant influence on the other three types of stability. Furthermore, the excitation system shows negligible influence on all types of phenomena. While the quadrature reactance shows negligible impacts on weak grid stability issues, reducing X'_q is shown to worsen swing dynamic oscillations.

In addition to the simulation studies, an explanation by use of the frequency-domain responses of the operational reactance is offered to elucidate the applicable frequency ranges of transient and subtransient reactance. The frequency-domain response of the terminal voltage vs. the excitation voltage of a SynCon is also examined to explain why the excitation system has negligible influence on stability.

Our contributions are threefold.

- We have demonstrated through EMT simulation that SynCons can enhance large- and small-signal stability in the subsynchronous region for power systems with IBR penetration.
- We offer a new perspective of the well-known operational reactances. We have shown that the direct and quadrature operational reactances are indeed non-diagonal components of a measured dq impedance matrix, influencing reactive and real current (power) respectively. This impedance has been used in stability analysis to demonstrate that a SynCon effectively reduces the equivalent grid impedance, thereby enhancing grid strength and improving stability associated with weak grid strength.
- We have also demonstrated and analyzed which parameters of a SynCon are most sensitive to a certain type of dynamics.

B. Structure

The rest of the paper is organized as follows. Section II presents how machine's various reactance is associated with the physical windings and the operational reactance's frequency-domain characteristics. Section II also shows the connection between the dq impedance of the SynCon and the operational reactances. Section III presents the testbed and introduces the stability scenarios as well as the impact of machine parameters on stability. Impedance-based stability

analysis results are presented in Section IV. Section V presents the effect of excitation systems on the stability issues. Finally, Section VI concludes this paper.

II. MACHINE REACTANCES & DQ IMPEDANCE

The synchronous condenser model is identical to synchronous machine model. In this research, a 20-MVA SynCon's model with typical parameters provided by the machine manufacturing industry is used for investigation. The parameters of the machine in per unit are shown in Table I.

TABLE I: SynCon parameters.

Parameters	Values
Rated power	20 MW
Rated Voltage	22 kV
Nominal freq.	60 Hz
X_d, X'_d, X''_d	1.683 pu, 0.19 pu, 0.14 pu
X_q, X'_q, X''_q	1.59 pu, 0.367 pu, 0.2 pu
X_{ls}, X_{md}, X_{mq}	0.11 pu, 1.53 pu, 1.48 pu
R_s	0.0045 pu
$T'_{q0}, T_{d0''}$	9.61 s, 0.04 s
$T''_{q0}, T_{q0''}$	2.5 s, 0.15 s
Inertia constant, Poles	2.12, 2
Friction factor	0.6

In machine analysis, operational impedance $X_d(p)$ is defined to relate the per unit flux linkage to the stator current (where p represents the derivative operator), as shown in Park's original paper [12]:

$$\psi_d = X_d(p)i_d. \quad (1)$$

The derivative operator p can be replaced by the Laplace transform variable s and $X_d(p)$ can be viewed as parallel branches connected with a series leakage reactance X_{ls} . Using s for p has been adopted later on by classic textbooks, e.g., [13]. Throughout this paper, s is the Laplace transform variable.

Fig. 1 shows the operational impedance at d -axis for a synchronous generator with a field winding and a damping winding in its rotor. Based on Fig. 1, the operational reactance can be expressed in the Laplace domain.

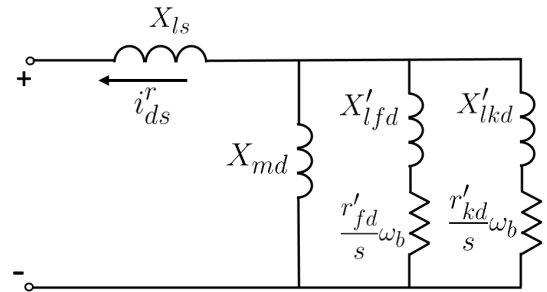


Fig. 1: Operational reactance of a synchronous machine. Note that s represents the Laplace transform variable.

The Bode diagram of the operational impedance of a field and damper winding in the d -axis reactance $X_d(s)$ is plotted in Fig. 2 for a SynCon.

It can be seen that X_d, X'_d and X''_d are referring to reactance associated to certain frequency ranges and their physical

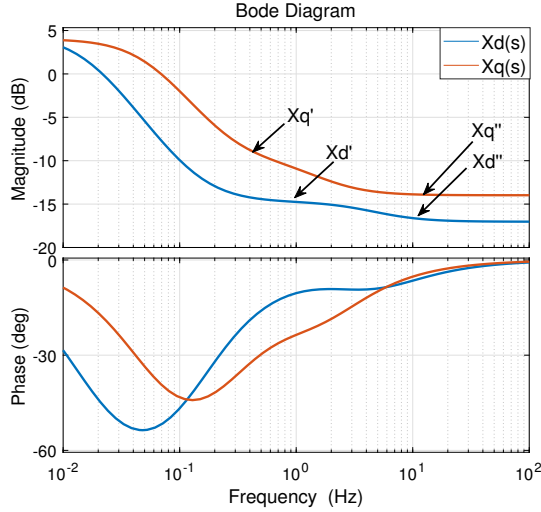


Fig. 2: Bode diagram of $X_d(s)$ and $X_q(s)$ versus frequency for the SynCon.

meanings are shown in Fig. 3. When $s = j0$, the field winding and damping winding branches are open circuited since r'_{fd}/s or r'_{kd}/s approach infinity. Hence, the steady-state reactance $X_d = X_{ls} + X_{md}$. When $s = j\infty$, r'_{fd}/s or r'_{kd}/s approach 0. The resulting reactance is X''_d . If the damping winding is not considered, and s approaches ∞ , the resulting reactance is X'_d .

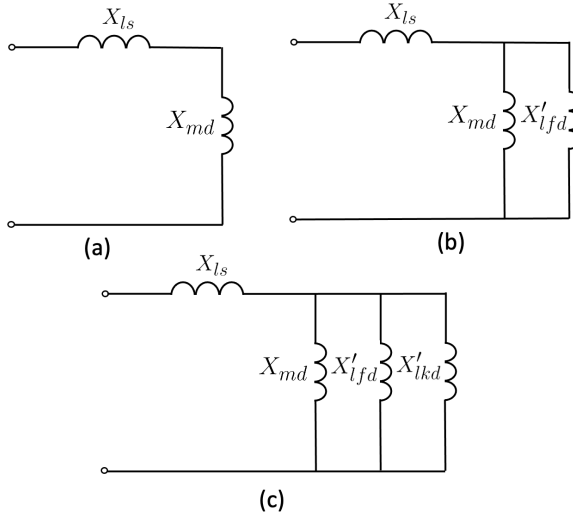


Fig. 3: (a) Synchronous reactance. (b) Transient reactance. (c) Sub-transient reactance. $X_{md} \gg X'_{afd} > X'_{ikd}$. Therefore $X_d \gg X'_d > X''_d$.

For this SynCon, the d -axis transient and subtransient open-circuit time constants T'_{d0} and T''_{d0} are 9.61 s and 0.04 s, respectively. If both time constants are associated to a first-order system, the bandwidths are 0.02 Hz and 4.6 Hz respectively. In the Bode diagram Fig. 2, it can be seen that $X_d(s)$ decreases from 1.68 pu to 0.19 pu when frequency increases from 0 Hz to about 1 Hz. X'_d corresponds to the value at 1.0 Hz while X''_d corresponds to the value above 9 Hz. In the region from 0.1 Hz to 3 Hz, $X_d(s)$ is closer to X'_d while in the region above 4.6 Hz, $X_d(s)$ is associated to X''_d .

This frequency-domain response of $X_d(s)$ helps speculate

the SynCon's behavior. At steady-state, the SynCon will behave as a reactance at the value of X_d or influenced by the magnetizing reactance X_{md} . During transients with frequency range below 4.6 Hz, the SynCon acts as X'_d or the field winding reactance X'_{afd} plays an active role. For rapid transient with frequency range above 9 Hz, the SynCon acts as X''_d or the damping winding's reactance X'_{ikd} plays an active role.

Similarly, the operational impedance $X_q(s)$ relates the per unit flux linkage of the quadrature axis to the quadrature stator current, and its expression can be found and plotted. It can be seen from Fig. 2 that in the frequency range of 1 Hz region, the reactance assumes the value of X'_q while in the 10 Hz above region, the reactance assumes the value of X''_q .

A. Connection with the DQ Impedance

In the recent decade, impedance-based stability analysis has become popular for IBR penetrated power grids [14], [15]. IBRs are often treated as black boxes since their control information is proprietary. An advantage of impedance-based analysis is that a device's impedance can be characterized through measurement experiments, e.g., frequency scan or transient data [16], [17]. When a three-phase IBR or generator is viewed from a synchronous rotating dq frame, their voltage and current variables are constant at steady state. Therefore, dq impedance has been popularly measured and used for analysis.

While the two operational reactances are well known for over a century since Park's introduction [12], how they are connected with the dq impedance viewed from a machine's terminal bus during operation has not been clarified in the literature. This subsection will fill the gap.

We start from the voltage and current relationship of a salient generator. The phasor diagram is shown in Fig. 4 [18]. For this phasor diagram, the d -axis is the rotor flux axis,

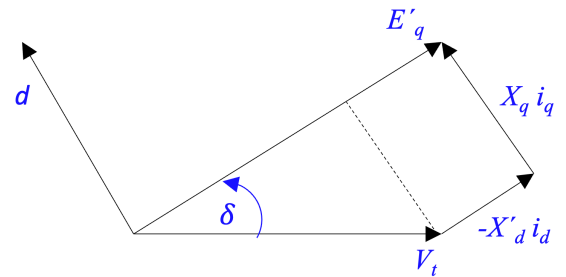


Fig. 4: Phasor diagram of a synchronous machine.

while the q -axis lags the d -axis by 90 degrees in the space and this axis aligns with the internal voltage's phasor. The terminal voltage (V_t), the currents (i_d and i_q), the internal voltage (E'_q), and the rotor angle (δ) can be related by the following equations:

$$E'_q = V_t \cos \delta - X'_d i_d \quad (2)$$

$$0 = -V_t \sin \delta + X_q i_q \quad (3)$$

If E'_q is treated as constant according to the assumption that flux linkage during transient is relatively constant, the small-

signal relationship between the terminal voltage and current can be written as follows:

$$\begin{bmatrix} \Delta V_{tq} \\ \Delta V_{td} \end{bmatrix} = - \begin{bmatrix} 0 & -X'_d \\ X_q & 0 \end{bmatrix} \begin{bmatrix} \Delta i_q \\ \Delta i_d \end{bmatrix} \quad (4)$$

It has to be noted that the dq in the machine is defined as the rotor's flux as d -axis, while the q -axis lags the d -axis by 90 degrees. On the other hand, in the conventional dq -frame definition adopted in [19], [20], the d -axis is usually aligned with a voltage space vector while the q -axis leads the d -axis by 90 degrees. The measured impedance or admittance of a device is usually based on this dq frame. This dq frame leads to straightforward understanding regarding a device's characteristics. Since the d -axis is aligned to the voltage space vector, a perturbation in the d -axis voltage is similar as a perturbation of the voltage magnitude; while a perturbation in the q -axis voltage is similar as a perturbation of the voltage phase angle. The resulting current responses also distinguish clearly the real and reactive current responses.

For a SynCon, since it delivers zero real power, its angle between the internal voltage and the terminal voltage is closed to 0 degree. Therefore, for a SynCon, the machine's q -axis is the measurement impedance's d -axis, while the machine's d -axis is the measurement impedance's q -axis. With this knowledge, we can see that the terminal voltage and the current flowing out of the machine in the measurement dq frame is as follows:

$$\begin{bmatrix} \Delta V_{td} \\ \Delta V_{tq} \end{bmatrix} = - \underbrace{\begin{bmatrix} 0 & -X'_d \\ X_q & 0 \end{bmatrix}}_{\mathbf{Z}_{dq}} \begin{bmatrix} \Delta i_d \\ \Delta i_q \end{bmatrix} \quad (5)$$

If the particular transient condition is extended to cover the entire frequency domain, and with the resistor effect ignored, the dq impedance or admittance of a machine for its own dynamics is as follows:

$$\mathbf{Z}_{dq}(s) = \begin{bmatrix} 0 & -X_d(s) \\ X_q(s) & 0 \end{bmatrix}, \mathbf{Y}_{dq}(s) = \begin{bmatrix} 0 & \frac{1}{X_q(s)} \\ \frac{-1}{X_d(s)} & 0 \end{bmatrix}. \quad (6)$$

We measure the admittance of the 20-MVA SynCon for verification. Since the operational impedances refer to the machine impedance of its own EMT dynamics, without consideration of the excitation dynamics and mechanical dynamics, we have disabled the SynCon's excitation system, and increased the SynCon's inertia by 1000 times. The SynCon is connected through a short impedance to a controllable voltage source and the dq voltages of the source are perturbed one after another. The dq currents to the machine are recorded. Fig. 5 shows the experiment data for the two experiments: v_d perturbation and v_q perturbation.

Based on the experiment data, the input/output systems are identified by use of system identification methods. In this case, we use MATLAB System Identification Toolbox's `tfest` function to identify the models which lead to output with high matching degree against the measurements. The resulting models' Bode diagrams are shown in Fig. 6. Remarks:

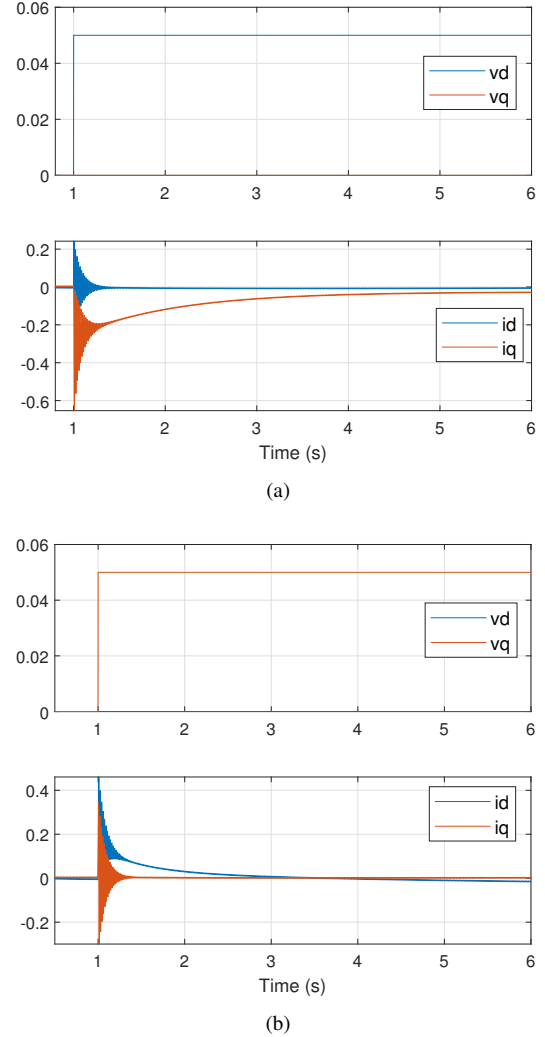


Fig. 5: (a) v_d perturbation. (b) v_q perturbation.

- The measured admittance components show resonance peaks at 60 Hz. This is due to the topology of the measurement testbed where two voltage sources are closely connected through a small inductive impedance. Such a circuit has a very small resistance and will show 60-Hz oscillations in the first half seconds for any excitation. This is a known phenomenon, as indicated in an influential reference [21].
- In the 0.01 Hz –20 Hz range, the measured Y_{qd} matches with $-1/X_d(s)$ excellently. The measured Y_{dq} matches with $1/X_q(s)$ in the frequency range of 0.1 Hz to 30 Hz.
- For the measured admittance, compared to the non-diagonal components, the magnitudes of the diagonal components in the below 20-Hz region can be ignored.

B. Projections of parameter influences

Eq. (6) connects the measured dq impedance/admittance and the operational reactances of a synchronous machine. It implicates that variation in the terminal voltage of a SynCon is correlated to the reactive current or reactive power through

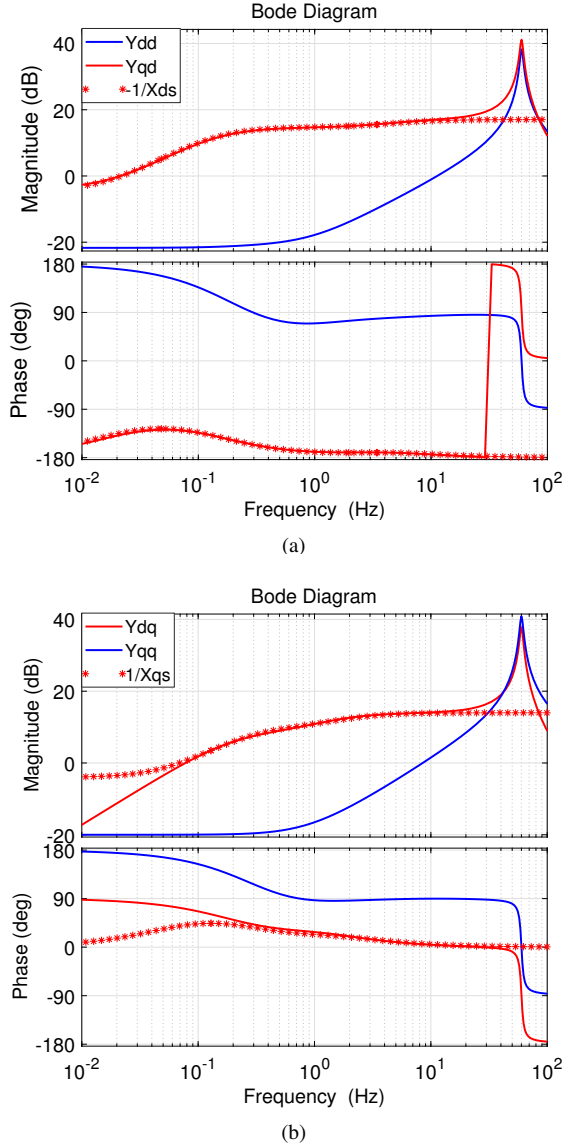


Fig. 6: (a) $X_d(s)$ validation. (b) $X_q(s)$ validation.

$X_d(s)$, while the variation in the phase angle is correlated to the real current or real power through $X_q(s)$.

These two relationships lead to the following projections.

(i) In order for the SynCon to be sensitive to terminal voltage variation and providing reactive power, a smaller $X_d(s)$ in the interested frequency region is preferred. (ii) $X_q(s)$ is not related to voltage and reactive power, therefore $X_q(s)$ plays negligible role in weak grid stability issues, which are mainly associated with voltage stability [4], [22]. On the other hand, a smaller $X_q(s)$ in the swing dynamic frequency range implicates that the machine's real power is more sensitive to angle change. This may lead to unwanted interactions with the swing dynamics.

III. IMPACT OF MACHINE REACTANCE ON STABILITY

In this section, sensitivity analysis results will be presented to examine various machine parameters on the SynCon's performance in stabilizing an IBR-penetrated system. Four

types of stability phenomena are created. The influence of a SynCon on these dynamics is examined one by one. While a type-4 wind farm is examined in this research and used in a test bed to create weak grid phenomena, similar weak grid phenomena can also be created using a type-3 wind farm or a solar PV farm to demonstrate SynCon's stability enhancement.

A. The test system and the dynamic phenomena

The single-line diagram of the test bed is shown in Fig. 7. This test bed is adapted from MATLAB/Simscap specialized power systems' demo type-4 wind farm built by Richard Gagnon and Jacques Brochu [23]. A 100-MW type-4 wind farm (the power base is 111 MW and therefore 0.9 pu corresponds to 100 MW) is connected to grid through a transmission network, its grid-side converter's control is to regulate the dc-link voltage V_{dc} and the reactive power or the point of common coupling (PCC) bus voltage. The transmission network consists of two parallel lines. A circuit breaker is located at one of the two lines to change the circuit SCR through switching on/off. The total transmission network impedance at the nominal frequency is $R_g + jX_g$, where R/X ratio is 0.1. A 20-MW 22-kV synchronous condenser (SynCon) is connected to the 220 kV bus through a transformer. This SynCon has a fast static exciter with an automatic voltage regulator equipped. The entire system can be viewed as two subsystems separated at the PCC bus: the wind farm and the grid. Note that the grid includes both the transmission systems and the SynCon.

When the synchronous condenser is not installed, upon a line tripping event, the wind farm may exhibit three types of scenarios: (i) 9-Hz oscillations, (ii) 3.7-Hz oscillations, and (iii) dynamic voltage stability. In addition, upon a grid voltage dip, the wind farm may be subject to PLL loss of synchronism (LOS).

In the dynamic voltage instability scenario, the system loses stability without oscillations and the characteristic feature is voltage collapse. These instability scenarios have been created by tuning the wind turbine grid-interconnected converter control parameters and control mode. Prior research on IBR weak grid stability in [24] has shown that weak grid stability can be understood by use of a feedback system consisting the blocks from the power measurement to the d -axis current through the d -axis outer control, the effect of d -axis current on the PCC bus angle, the PLL block (from the angle to the PLL angle), the effect of the PLL angle on the PCC bus voltage, and finally the effect of the PCC bus voltage to the power measurement. By use of the feedback system, it can be shown that if the q -axis outer control is in the ac voltage control mode, oscillations may appear when the stability limit is approaching. On the other hand, if the q -axis outer control is in the reactive power control mode, the system loses stability without oscillations. The influence of q -axis outer control on stability phenomena has been demonstrated in a hardware testbed [25]. Furthermore, this block diagram implicates that PLL's bandwidth and the d -axis outer control bandwidth influence the manifested oscillation's frequency.

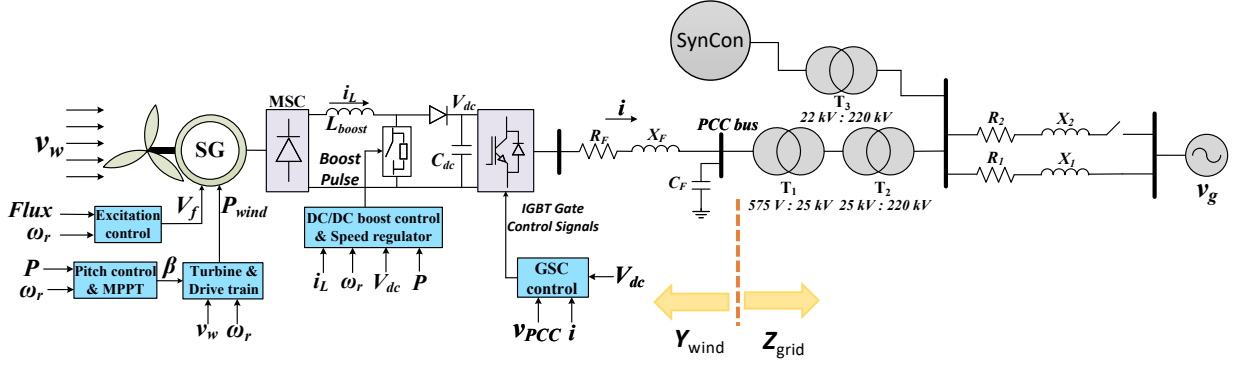


Fig. 7: The EMT test bed structure of a type-4 wind farm with a SynCon.

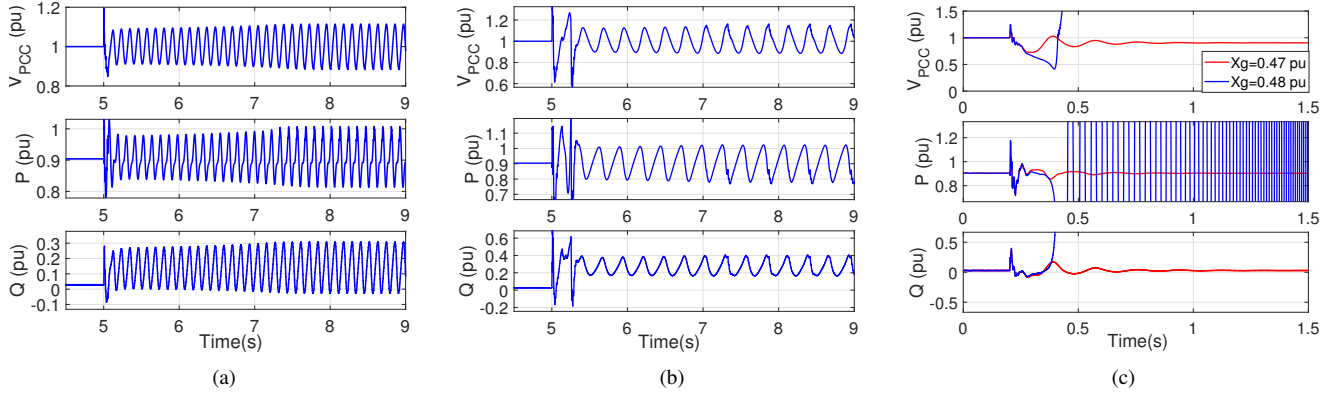


Fig. 8: A type-4 wind farm's dynamic performance after a line tripping event. (a) 9-Hz oscillations. (b) 3.7-Hz oscillations. (c) Dynamic voltage instability.

Therefore, two oscillation scenarios are created by assuming d -axis ac voltage control and q -axis dc voltage control, or V_{dc}/V_{ac} control. By making the dc voltage control and PLL faster, 9-Hz oscillations will appear after line tripping. By assuming d -axis ac voltage control and q -axis reactive power control, or V_{dc}/Q control, the dynamic voltage stability scenario is created. The parameters are shown in Table II.

TABLE II: Wind farm controller parameters for instability scenarios.

	V_{dc} controller	V_{ac}/Q controller	Current controller	PLL
PLL LOS	$1.1 + \frac{41.25}{s}$	$0.25 + \frac{25}{s}$	$0.4 + \frac{12}{s}$	$60 + \frac{1400}{s}$
9-Hz oscillations	$1.1 + \frac{412.5}{s}$	$0.25 + \frac{25}{s}$	$0.4 + \frac{48}{s}$	$60 + \frac{4480}{s}$
3-Hz oscillations	$1.1 + \frac{41.25}{s}$	$0.25 + \frac{25}{s}$	$0.4 + \frac{12}{s}$	$60 + \frac{1400}{s}$
voltage instability	$1.1 + \frac{412.5}{s}$	$0.25 + \frac{25}{s}$	$0.4 + \frac{48}{s}$	$60 + \frac{4480}{s}$

The EMT simulation results of the line tripping events are shown in Fig. 8. The wind farm is initially operating at steady-state and V_{PCC} is 1 pu. At $t = 5$ s, the line impedance has a step change and grid strength becomes weaker. In (a), the wind farm shows a 8.9 Hz oscillation when X_g changes to 0.42 pu, while in (b) the system shows a lower oscillation frequency as 3.7 Hz when X_g increases to 0.66 pu. In both (a) & (b), V_{dc}/V_{ac} control is deployed.

V_{dc}/Q control is deployed in Fig. 8 (c). In this condition, V_{ac} is regulated as 1 pu and Q as 0.05 pu, in which the operation condition is the same with V_{dc}/V_{ac} control. When X_g increases to 0.47 pu, the system recovers to stability after a couple of cycles. But if X_g increases to 0.48 pu, the system voltage collapses monotonically without any oscillations.

After adding the SynCon operating at 0 reactive power injection, the marginal conditions for the three scenarios have been changed. For scenario (a), the X_g 's margin changes from 0.42 pu to 0.69 pu; for scenario (b), X_g 's margin changes from 0.66 pu to 0.72 pu and the oscillation frequency changes from 3.7 Hz to 2 Hz; for scenario (c), X_g 's margin changes from 0.47 pu to 0.59 pu. In all three scenarios, with the addition of a SynCon, the system can operate in a weaker grid.

B. Influence of SynCon's direct-axis parameters

It is known that X_d , X'_d and X''_d can be adjusted by changing X_{md} , X'_{lfd} and X'_{lkd} . The winding resistance r'_{fd} and r'_{lkd} are also adjusted to ensure T'_{d0} and T''_{d0} intact. Based on the relation, three sets of parameters are investigated with varied X_d , X'_d and X''_d , separately. Table III lists the three sets of parameters and a base case is used for comparison. The machine parameter of the SynCon in the base case has a set of typical parameters. X_d in case 1 is only half of base case by reducing X_{md} . In case 2, X'_d decreases by reducing X'_{lfd} , and in case 3, X''_d decreases by reducing X'_{lkd} .

TABLE III: SynCon with different direct-axis winding parameters.

	X_{ls}	X_{md}	X'_{lfd}	X'_{lkd}	r'_{fd}	r'_{1kd}	X_d	X'_d	X''_d	T'_{d0}	T''_{d0}
Base case	0.11	1.573	0.0832	0.05	4.57e-4	0.008	1.683	0.19	0.14	9.61	0.04
Case 1	0.11	0.7865	0.0832	0.05	2.4e-4	0.008	0.897	0.19	0.14	9.61	0.04
Case 2	0.11	1.573	0.0277	0.05	4.4184e-4	0.005	1.683	0.137	0.13	9.61	0.04
Case 3	0.11	1.573	0.0832	0.005	4.57e-4	0.005	1.683	0.19	0.115	9.61	0.04

TABLE IV: SynCon with different quadrature-axis winding parameters.

	X_{ls}	X_{mq}	X'_{lkq1}	X'_{lkq2}	r'_{kq1}	r'_{kq2}	X_q	X'_q	X''_q	T'_{q0}	T''_{q0}
Base case	0.11	1.48	0.311	0.1385	0.0019	0.007	1.59	0.367	0.2	2.5	0.15
Case 1q	0.11	0.74	0.3937	0.1385	0.0016	0.007	0.85	0.367	0.2	2.5	0.15
Case 2q	0.11	1.48	0.1037	1.385	0.0017	0.0259	1.59	0.207	0.2	2.5	0.15
Case 3q	0.11	1.48	0.311	0.0277	0.0019	0.005	1.59	0.367	0.135	2.5	0.15

1) *Transient stability*: The first set of experiments is to compare SynCon's parameters on transient stability. The system is subject to 85% grid voltage dip lasting for 4 cycles, while X_g is 0.55 pu. The simulation results are shown in Fig. 9. The wind farm's PLL angle is shown to lose synchronism with the grid at the base case with the original SynCon parameters. It can be seen that case 1 and case 3 (reducing X_d or X'_d) have insignificant influence on improving transient stability, while case 2 (reducing X'_d) can avoid losing synchronism.

This experiment shows that X'_d is most sensitive to transient stability. It also confirms the conventional wisdom that X'_d is usually used in studying transient stability.

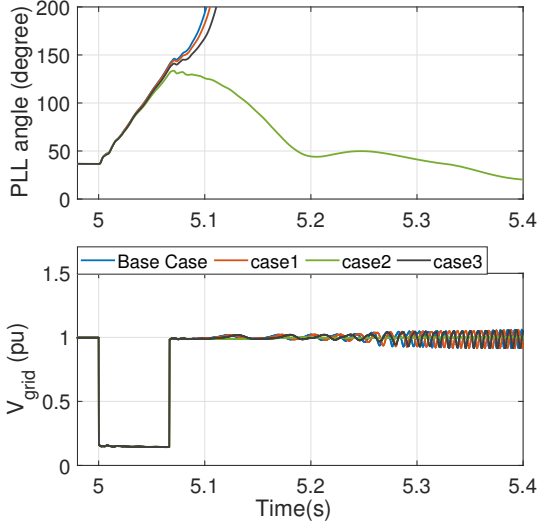


Fig. 9: EMT simulation results to show the effect of SynCon's parameters on PLL loss of synchronism transient stability.

2) *9-Hz oscillations*: To evaluate the impact of the parameters in wind farm's high frequency oscillations, at 5 s a line tripping event leads to the increase of X_g to 0.69 pu. Fig. 10 shows the system is subject to 9-Hz oscillation at base case, case 1, and case 2. It can be seen that neither reducing X_d nor reducing X'_d could improve the stability performance. On the other hand, when X''_d is reduced to 0.115 pu, the system is stable after the line tripping event. The results illustrate that the X''_d plays a role in high frequency oscillation condition.

It is also worthwhile to note that for case 3, even the 9-Hz oscillations have been damped out, the real power shows a

2-Hz mode. This mode is introduced by the SynCon and it becomes less damped when the grid becomes weak. Indeed, ERCOT's dynamic assessment report published in 2018 [26] has also noted about SynCon's electromechanical oscillation modes as a potential issue.

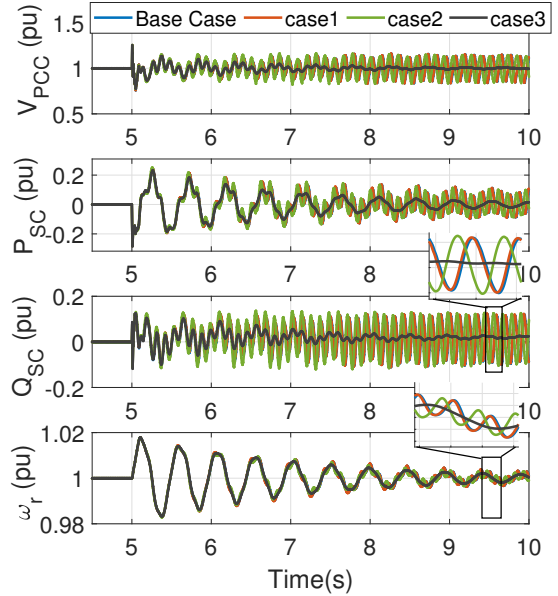


Fig. 10: EMT simulation results to show the effect of SynCon's parameters on the 9-Hz oscillations.

3) *2-Hz oscillations*: Without the SynCon, the wind farm is subject to 3.7-Hz oscillations, while with the SynCon the system is subject to 2-Hz oscillations when the grid strength reduces. This 2-Hz mode is related to the electromechanical mode of the SynCon. As shown in Fig. 11, when the transmission line is tripped at 10 s, the base case, case 1, and case 3 show sustained 2-Hz oscillations. However, in case 2, the oscillation is damped. This comparison illustrates that a lower X'_d could improve the stability performance while reducing X_d or X''_d has no impact for the low-frequency oscillation scenario.

4) *Dynamic voltage instability*: In this scenario, the system is tuned to lose stability instantly without any oscillation after X_g is increased to 0.59 pu. Fig. 12 shows the dynamic results subsequent to the event. As illustrated in Fig. 12(a) and (c), the system's performance is similar for the base case, case

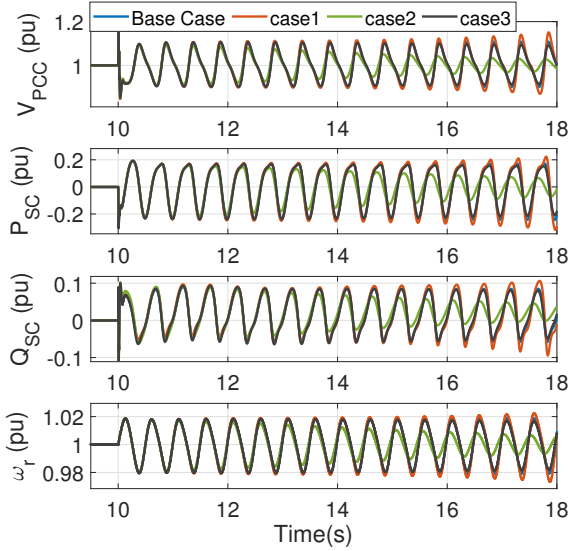


Fig. 11: EMT simulation results to show the effect of SynCon's parameters on the 2-Hz oscillations.

1 and case 3. In all three cases, the system becomes unstable within 0.5 s. However, in case 2, the system recovers stability as shown by Fig. 12(b). This experiment shows that reducing X'_d helps improve dynamic voltage stability.

In summary, for the above four types of stability scenarios, it can be seen that X_d has no influence, X'_d is most influential towards PLL synchronizing stability or transient stability, dynamic voltage stability and low-frequency oscillation stability. For rapid oscillations (e.g., 9-Hz oscillations), X''_d is the most influential factor.

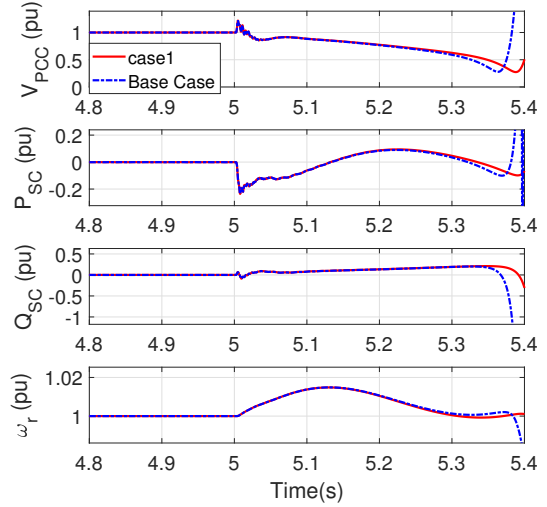
C. Influence of SynCon's quadrature-axis parameters

We have also carried out EMT simulation studies to examine SynCon's X_q , X'_q and X''_q variation on weak grid stability issues. Table IV shows the four cases' parameters. It is found that in general those parameters are insensitive to IBR weak grid stability. On the other hand, for 2-Hz swing dynamics related oscillations, reducing X'_q leads to worse performance.

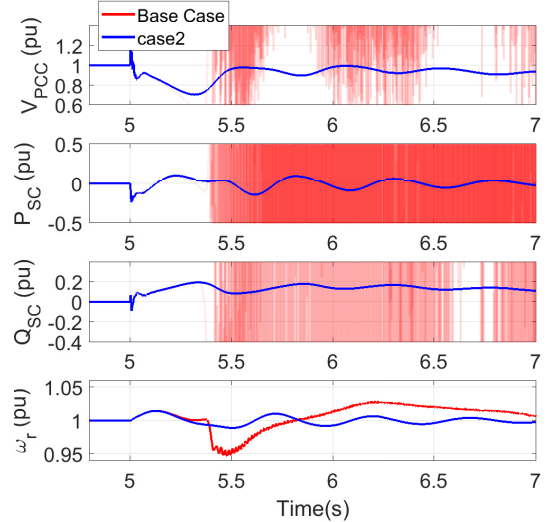
Fig. 13 shows the EMT simulation results for the testbed under the 2-Hz oscillation scenario. At $t = 1$ s, a line tripping event occurs, changing the grid impedance from 0.2 pu to 0.71 pu. It can be seen that reduction of X'_q (case 2q) leads to worse performance, while variation in X_q or X''_q has negligible impact. This observation aligns with the projection stated in Section II: a smaller $X_q(s)$ in the swing dynamic frequency region means that the real power is more sensitive towards angle variation. This may lead to poorer damping performance.

IV. EFFECT OF SYNCON ON EQUIVALENT IMPEDANCE & STABILITY ANALYSIS RESULTS

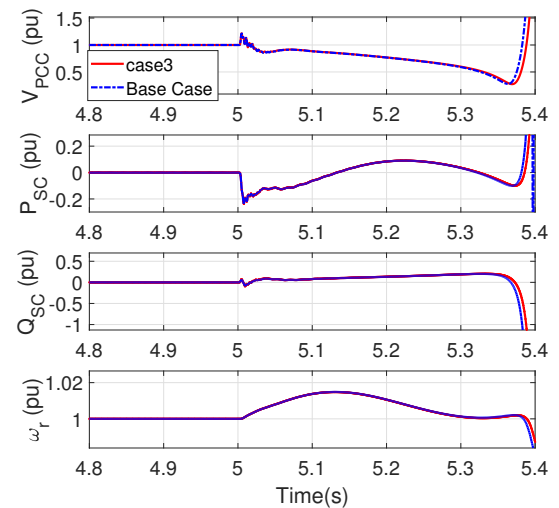
In this section, we present the effect of SynCon on the equivalent grid impedance and the stability analysis results for the wind farm integrated systems.



(a)



(b)



(c)

Fig. 12: V_{dc}/Q control wind farm with SynCon. (a) Case 1. (b) Case 2. (c) Case 3.

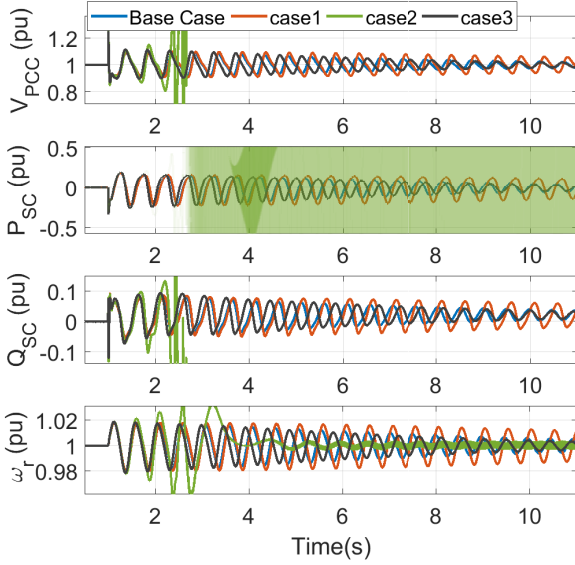


Fig. 13: EMT simulation results of the 2-Hz oscillations showing the effect of X_q , X'_q , and X''_q variation. case 1q: X_q reduction. case 2q: X'_q reduction. case 3q: X''_q reduction.

Our analysis in Section II has shown that that a SynCon mainly changes the nondiagonal components of a dq admittance/impedance. Additionally, $X_d(s)$ is correlated to Z_{dq} and Y_{qd} , while $X_q(s)$ is correlated to Z_{qd} and Y_{dq} .

Fig. 14(a) shows the equivalent grid impedance for five scenarios:

- When there is no SynCon, the grid impedance is a simple RL circuit's impedance.
- When there is a SynCon and the SynCon's parameters are its base case parameters.
- The SynCon's X_d is subject to reduction. This set is the case 1 parameters.
- The SynCon's X'_d is subject to reduction. This set is the case 2 parameters.
- The SynCon's X''_d is subject to reduction. This set is the case 3 parameters.

Fig. 14(b) shows the zoom-in of the dq component. It can be seen that a SynCon reduces the non-diagonal components of the equivalent grid impedance.

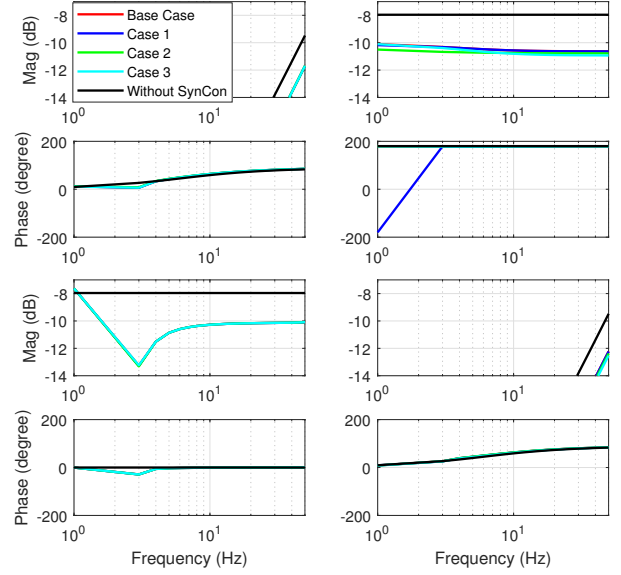
For stability check, the Nyquist plot of the determinant of $\mathbf{I} + \mathbf{Y}_{\text{wind}}\mathbf{Z}_{\text{grid}}$ is analyzed. The wind farm exporting current and its PCC voltage are associated with the wind farm's admittance \mathbf{Y}_{wind} . On the other hand, the voltage and the current are also associated with the grid impedance. Therefore:

$$\Delta \mathbf{I} = -\mathbf{Y}_{\text{wind}}\Delta \mathbf{V} = -\mathbf{Y}_{\text{wind}}\mathbf{Z}_{\text{grid}}\Delta \mathbf{I} \quad (7)$$

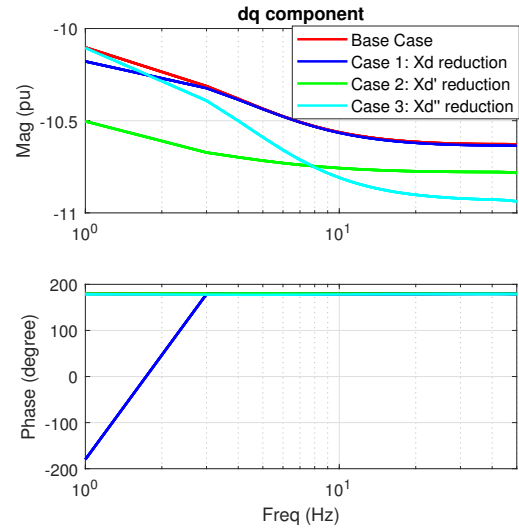
Therefore,

$$\Delta \mathbf{I} = (\mathbf{I} + \mathbf{Y}_{\text{wind}}\mathbf{Z}_{\text{grid}})^{-1}\Delta p, \quad (8)$$

where Δp notates a disturbance injected to the feedback system. It can be seen that the closed-loop system's stability is determined by the return matrix $\mathbf{I} + \mathbf{Y}_{\text{wind}}\mathbf{Z}_{\text{grid}}$. The roots of the determinant of this matrix are the closed-loop system eigenvalues. Therefore, the Nyquist plot of $|\mathbf{I} + \mathbf{Y}_{\text{wind}}\mathbf{Z}_{\text{grid}}|$



(a)



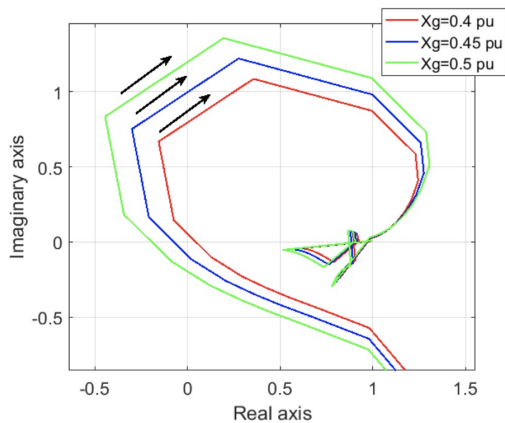
(b)

Fig. 14: The equivalent grid impedance. (a) dq -frame impedance. (b) zoom in of the dq component.

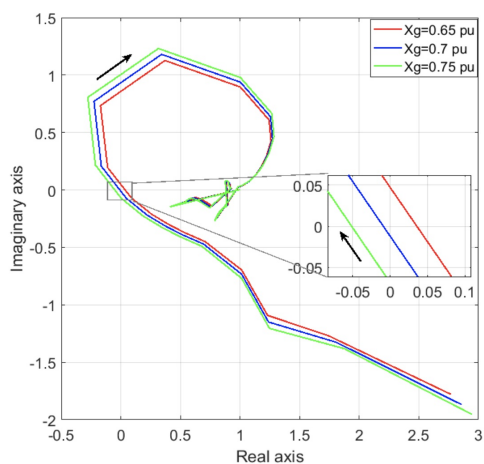
can be used to judge stability. If the diagram encircles $(0, 0)$, the system is unstable.

The wind farm's dq admittance can be measured and the detailed results can be found in our prior work [11], [27]. We use the wind farm parameters that can create 9-Hz oscillations for analysis. Fig. 15 shows the Nyquist plots for two scenarios: (a) without a SynCon, and (b) with a SynCon of base case parameters. It can be seen that without SynCon, when the transmission impedance X_g is 0.4 pu, the loci does not encircle $(0, 0)$, implicating a stable system. When X_g is 0.45 or 0.50 pu, the loci encircle $(0, 0)$, implicating instability. This analysis results align with the EMT simulation results shown in Fig. 8 which identifies the marginal condition as X_g at 0.42 pu.

With a SynCon, when X_g is 0.65 pu, the loci does not encircle (0,0), and when X_g is 0.7 pu or 0.75 pu, the loci encircle (0,0). The stability analysis results corroborate the simulation results in Fig. 10 which identifies the marginal condition as X_g at 0.69 pu.



(a)



(b)

Fig. 15: Nyquist diagrams of $|\mathbf{I} + \mathbf{Y}_{\text{wind}}\mathbf{Z}_{\text{grid}}|$. (a) Without SynCon. (b) With SynCon.

Finally, Fig. 16 shows the effect of SynCon's direct-axis reactance on the Nyquist plot of the $|\mathbf{I} + \mathbf{Y}_{\text{wind}}\mathbf{Z}_{\text{grid}}|$. It can be seen that at the condition of $X_g = 0.69$ pu, case 3 parameters lead to a stable system, effectively mitigating the 9-Hz oscillations, while the other two cases lead to unstable systems. This analysis result corroborates the EMT simulation results in Fig. 10 which implicating that X_d'' is the most effect parameter for 9-Hz oscillations.

V. IMPACT OF EXCITATION SYSTEM

We have shown that the machine's winding parameters influence stability. A question naturally arise: Does the excitation system have any impact on stability? In this section, this question is to be addressed.

An excitation system is used to provide direct current for the synchronous machine's field winding. The excitation systems are categorized as DC type, AC type and Static Excitation

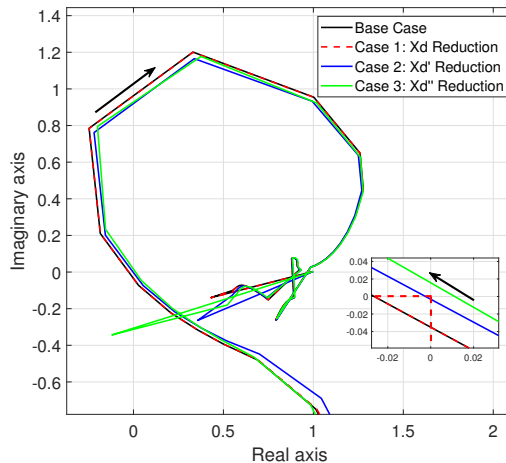


Fig. 16: Nyquist diagrams of $|\mathbf{I} + \mathbf{Y}_{\text{wind}}\mathbf{Z}_{\text{grid}}|$ when the SynCon's parameters are varied.

(ST) type according to IEEE standard [28]. In SynCons, fast static excitation systems are usually adopted.

Fig. 17 presents the block diagram of the excitation system. It consists of automatic voltage regulator to amplify to error between the V_t the machine terminal voltage and the sum of V_S power system stabilizer voltage and V^* the reference voltage. The output of the regulator's amplifier block $K_A/(1 + sT_A)$ is the input of the exciter. The exciter is modeled as a low-pass filter $1/(K_E + sT_E)$. For a fast static exciter, T_E is assumed as 0 and this block is a unit block. The time constants, T_B and T_C , are usually small enough to be neglected and could be made for zero. Saturation function is not considered in this model. The parameters of the excitation system are listed in Table V.

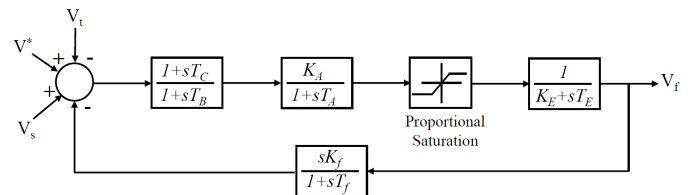


Fig. 17: The excitation system

TABLE V: Parameters of excitation system

Parameters	Value (SI)
T_C, T_B	0, 0
T_A, K_A	0.001, 300
T_E, K_E	0, 1
T_f, K_f	0.1, 0.001

The four dynamic cases will be examined again for excitation system with different voltage regulator gain K_A . Fig. 18 shows the effect of K_A on the system with base case. The grid impedance X_g experiences the same step change as the four scenarios created in the previous section. It can be seen that the dynamic performance when $K_A = 100$ and $K_A = 300$ are almost identical. This shows that K_A has insignificant influence on the system.

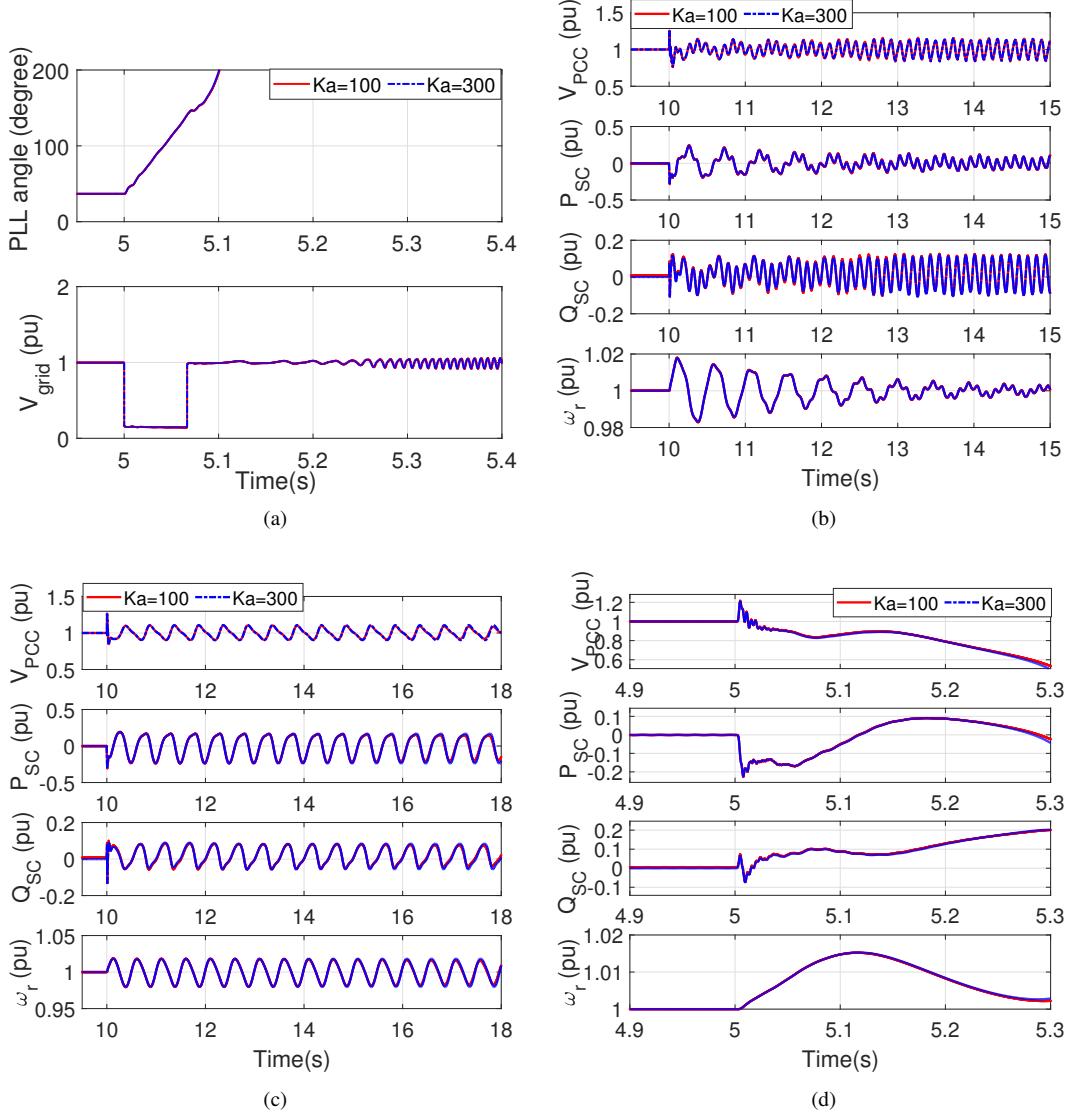


Fig. 18: Comparison of the voltage regulator gain K_a on dynamic performance. (a) Transient stability. (b) 9-Hz oscillations. (c) 2-Hz oscillations. (d) Dynamic voltage instability.

The above tests show that the excitation system has insignificant influence on all four scenarios. In the following, we examine why the excitation has no impact. Our study approach is to examine the frequency response of the excitation voltage on the terminal voltage, without any excitation system. The simplest relationship between the terminal voltage V_t and the excitation voltage viewed from the perspective of a stator E_{fd} can be found by ignoring the effect of stator current [18], [29] and it is same as a low-pass filter: $\frac{1}{T'_{d0}s+1}$, where T'_{d0} is the open-circuit time constant. With the consideration of the stator current, the effect of the grid impedance influences the transfer function and the transfer function becomes $\frac{K_3}{K_3T'_{d0}s+1}$, where $K_3 = \frac{X'_d+X_g}{X_d+X_g}$. If the grid is very strong, for this machine, K_3 is 0.167 and the low-pass filter's time constant becomes 1.5 seconds. The resulting bandwidth is 0.1 Hz. If the grid becomes weak, e.g., $X_g = 0.5$, the resulting bandwidth becomes even slower to 0.05 Hz.

We also use measurement data to understand this relationship. The SynCon is tested by disabling the excitation system. The input voltage V_f is set as a constant to ensure the same operation condition. Fig. 19 shows the terminal voltage response when input V_f has a 25% step change. The MATLAB command `tfest` is used to identify the system model. The comparison of measurement and estimated model's response demonstrates a high accuracy for the system identification.

The identified transfer function is as follows:

$$G(s) = \frac{0.01364s + 0.02594}{s^2 + 6.625s + 3.921} = \frac{0.526s + 1}{151(1.522s + 1)(0.168s + 1)} \quad (9)$$

Fig. 20 shows the Bode diagram of the transfer function. It can be seen that the bandwidth is about 0.1 Hz. Based on the above analysis result, the machine may be viewed as a low-pass filter from the excitation voltage to the terminal voltage. Since the

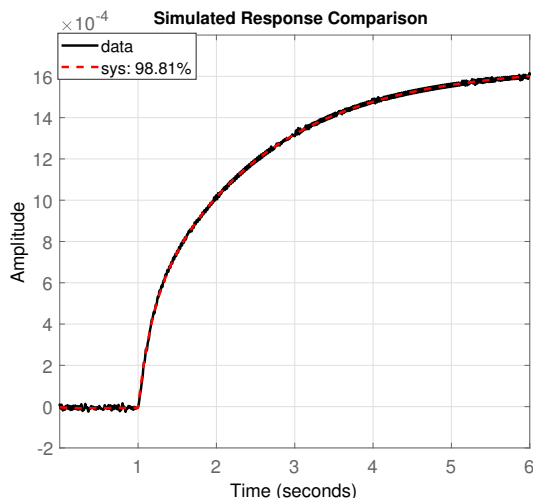


Fig. 19: The step response of the terminal voltage of the SynCon subject to a 25% increase in its v_f ; and the step response generated by the estimated model.

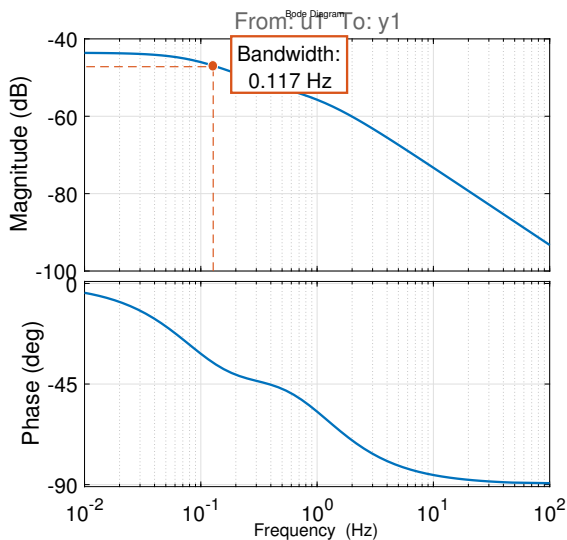


Fig. 20: The Bode diagram of the identified system $G(s)$ from the excitation voltage to the terminal voltage.

response is relatively slow, whatever how fast the excitation control is, the resulting terminal voltage response is limited by the machine characteristics. Therefore, the excitation system has no influence on the all four scenarios.

VI. CONCLUSION

The impact of SynCon's machine parameters and excitation system on stability of IBR-penetrated systems has not been rigorously examined in the literature. This paper fills the gap. Four stability scenarios have been investigated and they are transient stability (PLL loss of synchronism), dynamic voltage stability, low-frequency oscillations, and rapid high-frequency oscillations. It is found that SynCon's direct-axis transient reactance is the influencing factor for all types of stability scenarios, except the high-frequency oscillations. On the other hand, SynCon's direct-axis subtransient reactance

influences the rapid oscillations while imposing insignificant influence on the other types of stability scenarios. Due to slow voltage response of the machine, the excitation system imposes insignificant influence on the four types of stability. This paper offers an explanation of the observation by use of the operational impedance's frequency domain response. It is shown clearly that the steady-state, transient, and subtransient reactance correspond to the operational impedance of a certain frequency range. For majority of the system stability scenarios, it is seen that the transient reactance or the field winding inductance is the most influential factor.

ACKNOWLEDGEMENT

The authors would like to acknowledge Kay Chen, Robert Nelson and Carlos Grande-Moran for providing machine parameters and valuable feedback to this research.

REFERENCES

- [1] H. T. Nguyen, G. Yang, A. H. Nielsen, and P. H. Jensen, "Combination of synchronous condenser and synthetic inertia for frequency stability enhancement in low-inertia systems," *IEEE Transactions on Sustainable Energy*, vol. 10, no. 3, pp. 997–1005, 2019.
- [2] NERC, "Integrating InverterBased Resources into Low Short Circuit Strength Systems," North American Electric Reliability Corporation, Tech. Rep., 12 2017.
- [3] Joint NERC and Texas RE Staff Report, "Odessa Disturbance," North American Electric Reliability Corporation, Tech. Rep., September 2021.
- [4] Y. Cheng, L. Fan, J. Rose, S.-H. Huang, J. Schmall, X. Wang, X. Xie, J. Shair, J. R. Ramamurthy, N. Modi, C. Li, C. Wang, S. Shah, B. Pal, Z. Miao, A. Isaacs, J. Mahseredjian, and J. Zhou, "Real-world subsynchronous oscillation events in power grids with high penetrations of inverter-based resources," *IEEE Transactions on Power Systems*, vol. 38, no. 1, pp. 316–330, 2023.
- [5] L. Fan, Z. Miao, S. Shah, Y. Cheng, J. Rose, S.-H. Huang, B. Pal, X. Xie, N. Modi, S. Wang *et al.*, "Real-world 20-hz ibr subsynchronous oscillations: Signatures and mechanism analysis," *IEEE Transactions on Energy Conversion*, vol. 37, no. 4, pp. 2863–2873, 2022.
- [6] Y. Li, L. Fan, and Z. Miao, "Stability control for wind in weak grids," *IEEE Trans. Sustainable Energy*, vol. 10, no. 4, pp. 2094–2103, 2019.
- [7] L. Fan, Z. Wang, and Z. Miao, "Large angle deviation in grid-following IBRs upon grid voltage dip," *IEEE Transactions on Energy Conversion*, pp. 1–10, 2023.
- [8] A. Karisik, W. Ong, T. Bertes, T. Lim, and J. Leung, "Installation of a synchronous condenser - the kiamal solar farm example," in *2021 IEEE PES Innovative Smart Grid Technologies - Asia (ISGT Asia)*, 2021, pp. 1–5.
- [9] Potomac Economics, "2018 state of the market report for the ERCOT electricity markets," Tech. Rep., June 2019.
- [10] Y. Cheng and S. Huang, "Strengthening the West Texas Grid to Mitigate Widespread Inverter-Based Events – Operation Assessment Results," ERCOT, Tech. Rep., Feb 2023.
- [11] L. Bao, L. Fan, and Z. Miao, "Wind farms in weak grids stability enhancement: Syncon or statcom?" *Electric Power Systems Research*, vol. 202, p. 107623, 2022. [Online]. Available: <https://www.sciencedirect.com/science/article/pii/S0378779621006040>
- [12] R. H. Park, "Two-reaction theory of synchronous machines generalized method of analysis-part i," *Transactions of the American Institute of Electrical Engineers*, vol. 48, no. 3, pp. 716–727, 1929.
- [13] P. C. Krause, O. Wasynczuk, S. D. Sudhoff, and S. Pekarek, *Analysis of electric machinery and drive systems*. Wiley Online Library, 2002, vol. 2.
- [14] J. Sun, "Impedance-based stability criterion for grid-connected inverters," *IEEE transactions on power electronics*, vol. 26, no. 11, pp. 3075–3078, 2011.
- [15] L. Fan and Z. Miao, "Admittance-based stability analysis: Bode plots, nyquist diagrams or eigenvalue analysis?" *IEEE Transactions on Power Systems*, vol. 35, no. 4, pp. 3312–3315, 2020.
- [16] L. Fan, Z. Miao, P. Koralewicz, S. Shah, and V. Gevorgian, "Identifying dq-domain admittance models of a 2.3-mva commercial grid-following inverter via frequency-domain and time-domain data," *IEEE Transactions on Energy Conversion*, vol. 36, no. 3, pp. 2463–2472, 2020.

- [17] L. Fan and Z. Miao, "Time-domain measurement-based dq -frame admittance model identification for inverter-based resources," *IEEE Transactions on Power Systems*, vol. 36, no. 3, pp. 2211–2221, 2020.
- [18] A. R. Bergen, *Power systems analysis*. Prentice Hall, 1986.
- [19] A. Yazdani and R. Iravani, *Voltage-sourced converters in power systems: modeling, control, and applications*. John Wiley & Sons, 2010.
- [20] L. Fan and Z. Miao, *Modeling and Stability Analysis of Inverter-Based Resources*. CRC Press, 2023.
- [21] L. Zhang, L. Harnfors, and H.-P. Nee, "Power-synchronization control of grid-connected voltage-source converters," *IEEE Transactions on Power systems*, vol. 25, no. 2, pp. 809–820, 2009.
- [22] L. Fan and Z. Miao, "An explanation of oscillations due to wind power plants weak grid interconnection," *IEEE trans. Sustainable Energy*, vol. 9, no. 1, pp. 488–490, 2018.
- [23] R. Gagnon and J. Brochu, "MATLAB/Simscap: Wind Farm - Synchronous Generator and Full Scale Converter (Type 4) Average Model."
- [24] L. Fan, "Modeling type-4 wind in weak grids," *IEEE trans. Sustainable Energy*, vol. 10, no. 2, pp. 853–864, 2019.
- [25] L. Bao, L. Fan, Z. Miao, and Z. Wang, "Hardware demonstration of weak grid oscillations in grid-following converters," in *2021 North American Power Symposium (NAPS)*. IEEE, 2021, pp. 01–06.
- [26] E. Rehman, M. Miller, J. Schmall, and S. H. Huang, "Dynamic Stability Assessment of High Penetration of Renewable Generation in the ERCOT Grid," ERCOT, Tech. Rep., Apr 2018.
- [27] L. Fan, Z. Miao, L. Bao, S. Shah, and R. H. Ramakrishna, "Dq admittance model extraction for IBRs via gaussian pulse excitation," *IEEE Transactions on Power Systems*, vol. 38, no. 3, pp. 2966–2969, 2023.
- [28] "IEEE recommended practice for excitation system models for power system stability studies," *IEEE Std 421.5-2016 (Revision of IEEE Std 421.5-2005)*, pp. 1–207, 2016.
- [29] L. Fan, *Control and dynamics in power systems and microgrids*. CRC Press, 2017.



Zhixin Miao (Senior Member, IEEE) received the B.S.E.E. degree from the Huazhong University of Science and Technology, Wuhan, China, in 1992, the M.S.E.E. degree from the Graduate School, Nanjing Automation Research Institute (Nanjing, China) in 1997, and the Ph.D. degree in electrical engineering from West Virginia University, Morgantown, in 2002.

Currently, he is a full professor at the University of South Florida (USF), Tampa. Prior to joining USF in 2009, he was with the Transmission Asset Management Department with Midwest ISO, St. Paul, MN, from 2002 to 2009. His research interests include power system stability, microgrids, and renewable energy. Dr. Miao serves as an associate editor for *IEEE trans. Sustainable Energy*.



Li Bao received the B.S. degree in electrical engineering from Northwestern Polytechnical University, Xi'an, China, in 2015, M.S. and Ph.D. degrees in electrical engineering from University of South Florida, Tampa, FL, USA, in 2016 and 2022. Currently, he is a senior engineer at Eversource Energy focusing on electromagnetic transient simulation and analysis of offshore wind farm grid integration.



Lingling Fan (Fellow, IEEE) received the B.S. and M.S. degrees in electrical engineering from Southeast University, Nanjing, China, in 1994 and 1997, respectively, and the Ph.D. degree in electrical engineering from West Virginia University, Morgantown, in 2001.

Currently, she is a full professor with the University of South Florida, Tampa, where she has been since 2009. She was a Senior Engineer in the Transmission Asset Management Department, Midwest ISO, St. Paul, MN, from 2001 to 2007, and an Assistant Professor with North Dakota State University, Fargo, from 2007 to 2009. Her research interests include power systems and power electronics. Dr. Fan serves as Editor-in-Chief for *IEEE Electrification Magazine* and Associate Editor for *IEEE trans. Energy Conversion*.